MACHINE LEARNING-DRIVEN PARAMETRIC ANALYSIS OF ECO-FRIENDLY ULTRASONIC WELDING FOR AL6061-CU ALLOY JOINTS

A. Karan[1], S. Arungalai Vendan[1*], M. R. Nagaraj[2], M. Chaturvedi[1], S. Sivadharmaraj[3]

[1]Department of Electronics and Communication, Dayananda Sagar University, Bangalore, India
[2]Department of Mechanical Engineering, Sir Krishna College of Technology, Coimbatore, India
[3]Department of ISE, New Horizon College of Engineering, Bangalore, India
Corresponding Author: arungalai-ece@dsu.edu.in

ABSTRACT

This study outlines the research conducted to examine the mechanical behaviour and microstructural characteristics of Al-Cu dissimilar wires joints welded using ultrasonic joining process that commonly finds application in automotive components, heat exchangers and electrical home and industrial appliances. The primary focus is on the metallurgical transformations to evaluate the pattern of molecular diffusion and spread within the weld, the consistency of diffusion, and the resulting alterations in strength caused by ultrasonic vibrational heat. This procedure entails conducting experimental trials to join the wire materials according to per design of experiments, wherein the process parameters significantly influencing the output are systematically varied, and consequently, subjecting the joints to shear testing. Subsequently, the welded specimens undergo microscopic examination and the images are captured using image analysers. In addition, scanning electron microscopy (SEM) pictures are examined to gain insights into the surface shape and assess the degree of weld production and performance. The findings demonstrate a direct correlation between the vibrational temperature and the weld strength. In addition, the joint surface exhibits a consistent weld pattern in the majority of the samples, with just a few instances of inconsistencies when the trail is carried out at low heat input. Electrical resistance at the joints is measured to understand the electrical parametric variations if any due to process parameters. A machine learning tool is employed to forecast the weld strength and joint resistance for differing ranges of process parametric values and accordingly optimize it.

KEYWORDS: Al-Cu dissimilar joints, ultrasonic welding, electrical resistance, machine learning, heat

1. INTRODUCTION

Hybrid engineering structures and components are the focus of manufacturing technology, where joining light weight material alloys is crucial. Lightweight components for automotive and aerospace applications are the focus of current engineering trends, which will help to achieve the objective of developing an adaptable product. Under these conditions, it is imperative to assess the capability to weld such a variety of lightweight materials like aluminium and copper to create flawless structural components and designs. Ultrasonic welding bonds materials without melting them by creating frictional heat with high-frequency ultrasonic vibrations. Vibrational force between the weld surfaces breaks down and scatters molecules and thin oxide coatings into the two faying surfaces during mechanical mixing. Ultrasonic waves cause compressive deformation. Several researchers have demonstrated ultrasonic welding results for aluminum and copper. The settings used in dissimilar ultrasonic spot welding (USW) for the joining of 3003 aluminum alloys with 304 stainless steel were optimized by Shakil, M., et al. [1]. In order to investigate the development of intermetallic compounds (IMCs) in relation to weld time, Yang, J.W., et al. used ultrasonic welding to conduct dissimilar junctions on copper and aluminum [2]. By ultrasonically connecting copper and aluminum metals with and without a zinc interlayer, Balasundaram, R., et al. conducted research on the zinc interlayer. Greater tensile strength was shown by the Zn interlayer weld [3]. Ji, H., et al. looked at how 1100 aluminum foils bonded by ultrasonic metal welding (UMW) were

Date of submission/acceptance: 31.05.2024/15.12.2024
http://doi.org/10.35219/awet.2024.04

affected by oscillation amplitude and deformation reduction [4]. Using a tensile shear strength test, Fujiia, H.T., et al. studied the weld properties of the 1050 aluminum alloy with copper joined by USW [5]. A study was conducted on the microstructural analysis, mechanical properties, and effects of time and aging on Al alloy 6111 and TiAl6V4 joined using Power Ultrasonic Spot Welding by Zhang, C.Q., et al [6]. To analyze the microstructure as well as the mechanical attributes of welding copper to AZ31B magnesium alloy, Macwan, A., et al. conducted USW at different energy levels [7]. The dissimilar junctions of Al to HSLA steel were examined by Patel, V.K., et al. for the variations in the microstructure, fatigue capacity, and shear tensile strength. Two non-uniform sub-surface layers are seen: the Al-Zn eutectic layer and the thin IMC layer of Al and Fe [8]. The analysis of dissimilar metal welding (mild steel and Al 5052 alloy) was done by Sasaki, T., et al. utilizing a variety of weld surfaces, including curved and knurled weld tips (K-tip) with or without knurled edges (C-tip) [9]. In order to improve the weld strength, Satpathy, M.P., et al. created specific horns, and Ansys is used to analyze length [10]. In order to characterize the microstructure, Wu, X., et al. ultrasonically welded three layers of lithium-ion battery tabs (Al or Cu) and examined their failures [11]. In order to combine AA6061 with pure copper, Yang, J., et al. conducted a comparison study between ultrasonic welding and resistance heat assisted ultrasonic welding [12]. Using a specifically designed horn (four-point tips) for ultrasonic welding, Seo et al. performed the welding of Ni and Cu sheets [13]. Using bond density data, Lee, S.S., et al. studied the effective configuration of the tool for multilayer ultrasonic welding [14]. Zhang, G., et al. joined Al ribbon and Cu sheet using ultrasonic welding and examined the microstructure and fracture properties of the materials [15]. Using genetic algorithms (GA) and fuzzy logic, Satpathy, M.P., et al. optimized parameter combinations for ultrasonically welded brass UNS C27000 sheet and AA1100 ultrasonically welded sheets [16]. They also built a non-linear second order regression model. Using power ultrasonic spot welding, Haddadi, F., et al. investigated the weld properties of Al 6111-T4 and zinc-coated steel [17]. Spot welding of Al with galvanized high strength-low alloy and low carbon steel sheets was carried out with ultrasonic welding by Mizra, F.A., et al. FeAl3's IMC layer development is discovered when its microstructure, tensile, and fatigue properties are examined. [18]. Al and Cu plates were ultrasonically welded by Asami et al. using vibration and a planar focus, and the weld strength was measured to evaluate the welding features [19]. In order to forecast the thermal gradient in ultrasonically welded materials such as magnesium (AZ31), low carbon steel (Dc04), and AA6111, Jedrasiak, P., et al. published a FEM [20]. Because it might be difficult to have adequate control over grain size and mechanical properties, Kicukov, E., et al. presented a review on ultrasonic welding of dissimilar materials [21]. The effect of vibration amplitude and weld time on the weld strength of Al alloys that are similar and are ultrasonically welded was investigated by Shin et al. [22]. Ultrasonic spot welding of aluminium (AA6111 and 7055) to different alloys of low carbon steel (DC04) was carried out by Xu, L., et al. [23]. The impact of interfacial response on the mechanical properties was examined. For copper and aluminium that were ultrasonically welded, Ni, Z., et al. found that the hardness of the aluminium decreased while an increase was noted in the energy and tensile strength [24]. Copper and aluminium weld specimens with a T-peel failure load and elevated tensile shear were investigated by Satpathy, M.P. et al [25]. The joining of dissimilar materials, AA2139-TiAlV4, was examined by Zhang, C.Q., et al. They found that as the weld time increases, so does the fracture energy of the welds and peak load [26]. Sridharan et al. used a 9kW ultrasonic additive manufacturing machine to conduct electron back scatter on aluminium-titanium. Severe shear deformation at the weld contact is the foundation of the weld production mechanism [27]. In order to design the microstructural and temperature-dependent mechanical deformation for the ultrasonic spot welding process, Shen, Ninggang, et al. created a metallo-thermo-mechanically coupled model [28]. Using USW, Higashi et al. assessed the Mg-Zn-Y alloy's weldability and the mechanism of microstructure development [29]. Under the combined influence of ultrasonic energy and compression force, Chen et al. conducted ultrasonic welding for specimens made of copper and aluminium [30]. The effects of vibration amplitude, weld time, and weld pressure were analysed by Satpathy, M. P., et al. and compared using microstructure analysis and the T-peel and tensile shear test [31]. In order to forecast energy absorption capacity, peak shear load, and failure mechanisms for ultrasonic metal welds of copper and aluminium, Banu, Mihaela, et al. describes weld performance models [32]. Al-Cu joints, Al-AISI 304 steel, and Al-UNS C27000 brass combinations were tested by Satpathy, M.P., et al. The formation of Al2Cu, Cu5Zn8, and FeAl3 IMC has been seen [33]. Aluminium to copper was welded ultrasonically using an Al2219 particle interlayer by Ni, Z. L., and F. X. Yet al [34]. Friction stir welding of Al-Cu for post-weld cold rolling (PWCR) and annealing treatments was studied by Deng, Qinghong, et al. [35]. The lap shear tensile strength of ultrasonic spot-welded Al-Cu joints using Al2219 alloy particles as the interlayer was studied by Ni, Z. L., et al. [36]. In order to acquire the mechanical and microstructural characterisation, Zhou, X., et al. examined the Al-Cu brazing zone and the Al-Al welding region [37]. The interfacial connection between two different zinc-coated steels, hot-dipped DX56-Z and galvannealed DX53-ZF, and aluminium 6111-T4 was examined by Haddadi, F. [38]. To manage the longitudinal-torsion vibration of the vibrating source, Asami, T., et al. created a new planar

locus based ultrasonic vibration source [39, 40]. Bergmann, J.P., et al. used ultrasonic welding to examine the effects of interface behaviour on the diffusion mechanism and joint parameters in an Al-Cu welded specimen [41]. In order to get around the difficulties of welding dissimilar sheets of conductive multi-metals for EV (Electric Vehicle) applications, Lee, S.S., et al. used ultrasonic welding of dissimilar metals [42]. Discrete mass-spring-damper models were developed by Kang, B., et al. [43] to identify the dynamics and vibrations associated with ultrasonic welding. In their investigation of the Al-epoxy interfacial region for ultrasonically attached matrix composite consisting of carbon fibre reinforced epoxy resin to AA5754 sheets, Lionetto, F., et al. observed pores and fissures caused by plastic deformation [44]. Through the use of statistical classification processes, Lee, S.S., et al. developed a quality monitoring system to identify control components during the ultrasonic welding of Li-ion batteries in automotive applications. A link between the USW signal, joint performance, and process circumstances was demonstrated by the authors [45]. The effects of lap configuration on the mechanical characteristics and microstructure of Cu-Al and Al-Cu joints were studied by Regensburg, A., et al. The effects of locally preheating the specimen on the horn to promote wire deformation at the interface were also presented by the author [46, 47]. Using ultrasonic additive manufacturing (UAM), Li, J., et al. suggested a novel fabrication technique to create metal matrix composite (MMC) structures [48]. Using the Taguchi approach, Khan, U., et al. developed an efficient procedure to resolve optimal welding to maximize the weld strength produced by ultrasonic welding of Al-Cu [49]. Using TEM, Zhang, Z., et al. examined the phases and microstructure at the junction of Al-Cu sheets welded using the USW technique. The effects of interlayer on the mechanical characteristics and microstructure of Ti6Al4V and Al6061 alloys that were ultrasonically welded were examined by the author [50, 51]. The effects of weld energy on the mechanical and microstructural properties of pure Cu plates that were ultrasonically connected were investigated by Yang, J., et al. [52]. Peng, H., et al. assessed the fatigue resistance, microstructures, and single lap shear of Al6022-T43 alloys that were ultrasonically welded at various energy levels [53]. The parametric effects of vibration amplitude, weld time, and weld pressure during ultrasonic welding of Cu C10100 and AA1100 alloys were described by Satpathy, M.P., et al. [54]. The microstructural, mechanical characteristics, and impacts of vibrational amplitude of ultrasonically connected Al-Cu joints were examined by Liu, G., et al. Energy-dispersive X-ray spectroscopy (EDS) and XRD are used to identify the production of IMC layers [55, 56]. The electrical resistance and performance of Al-Cu sheets that are ultrasonically bonded in several layers are analysed. Joint electrical resistance is used to validate the quality of the Cu-Al battery cell joint [57]. Macwan, A., et al. investigated the joining of AA6111-T4 and HSLA steel by ultrasonic welding at different energy levels [58]. Ren, D., et al. looked into the use of ultrasonic spot welding for combining incompatible metals (titanium and magnesium alloys) [59]. Using a range of welding conditions, Satpathy, M.P., et al evaluated changes in microstructure, weld strength, and interfacial response in ultrasonically welded Cu UNS C10100 and Stainless steel 304 with brass interlayer [60]. Balogh, M.P., et al worked on a welding assembly that had a reliable controller. The controller governed the clamping of the sonotrode to the cleaning block and ensured transmission of ultrasonic energy to the cleaning block for a defined duration adequate for the removal of residual amounts of metal from the welding pads of the sonotrode [61]. The oscillation pattern of the components to be joined by ultrasonic welding can provide information regarding how the pieces are fixed in the machine and the quality of the weld, according to Mostafavi, S., et al. The oscillations' frequency spectrum reveals that, although the obvious changes in shape do not appear to have a significant impact on the oscillations, terminal fixations during the ultrasonic welding process significantly change the vibration pattern [62]. Cai, W. et al discuss about Adaptive control technology, data depth fusion, intelligent multi-sensor signal acquisition platforms, and other possible research issues and challenges based on real-time intelligent monitoring [66]. Eren, B. et al explain about the usage of artificial intelligence (AI) tools to anticipate and optimize the FSW process parameters for maximum cost-effectiveness and good quality [67]. Tsuzuki, R. et al summarize the current state of the engineering plan, as well as upcoming automation and artificial intelligence technologies, for the Digital Smart Factory's welding and inspection procedures in the aerospace sector [68]. Cardellicchio, A. et al proposes an automated flaw identification technique based on lightweight machine learning techniques, as well as a high-throughput laser profilometry data collection and processing system [69].

Several reports are available on ultrasonic welding of dissimilar materials. The reported results offer an understanding of parametric dependencies and also can be utilised as a database for process parametric variations for the joining of some geometries of dissimilar materials. However, the reports on ultrasonic joining of thin wires made of dissimilar Al-Cu alloys are few in number, while this material has greater potential for deployment in electrical and automobile applications. The application of machine learning tools for data training based on experimentation and subsequent parametric forecasting is unexplored for ultrasonic dissimilar joints. The experimental study and machine learning-based parametric analysis of ultrasonic welding for connecting dissimilar metals offer substantial improvements over conventional approaches. Traditional parametric analysis uses empirical models and trial-and-error, which is time-consuming and

inaccurate. However, machine learning algorithms may find complex patterns and correlations between welding parameters and outcomes in large datasets. Prediction accuracy, welding conditions, and joint quality improve with this method. This work uses experimental data and machine learning to improve ultrasonic welding for faster, more reliable, and higher-quality metal joining.

2. MATERIALS AND METHODS

This investigation focuses on conducting ultrasonic welding of Cu alloy and Al6061 wires by varying the process parameters based on the design of experiments. Various industrial applications necessitate the joining of dissimilar metallic wires. The ultrasonic welding machine utilized in this study is characterized by a power rating of 10kW and is identified by the model (UWMM 1000), as depicted in Figure 1.

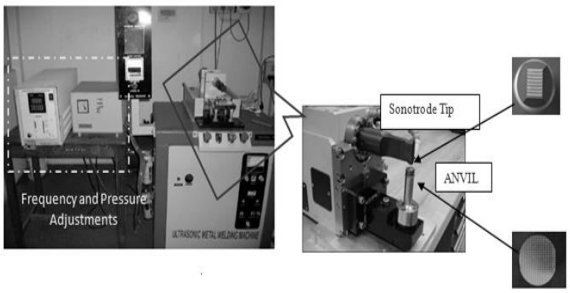

Fig. 1. An ultrasonic welding equipment is utilised to join aluminum-copper wires.

Al6061 and Cu wires with diameter of 0.5 mm is used for the experimentation and 30 trails are run using predetermined settings.

In ultrasonic spot welding (USW), high-frequency vibrations heat the contact. Heat shrinks weld yield strength and increases plastic deformation, creating localized adhesion and micro-joints that strengthen bonding. Ultrasonic spot welders have five main parts: a high-frequency power supply (20 kHz), a piezoelectric transducer that converts electrical to mechanical vibrations, a wedge that amplifies these vibrations, a reed that transfers energy to the metal, and a pneumatic cylinder that clamps. Heat generation depends on interfacial shear stress. The sonotrode descends during welding because relative movement, pressure, and vibration squeeze materials between ridges. With extended welding periods, this method transfers most aluminum oxide layers, resulting in direct Al/Cu welds at several interfaces.

Ultrasonic welding parameters include time, vibration amplitude, and clamping pressure. Due to continual scouring, excessive welding time can develop cracks and weaken joints. Documenting these elements' interdependency is crucial. High vibration amplitude increases surface deformation and scrubbing, improving weldability. However, excessive clamping pressure increases friction, limiting joint strength and relative motion. High-quality joints require energy in a short period. Overuse of ultrasonic energy can cause tip sticking or fatigue fractures.

Ultrasonic welding thin aluminum and copper wires is challenging. These metals have different mechanical and thermal properties, which might affect weld quality. Thin wires risk thermal damage, fatigue cracks, and poor bonding. Copper's high thermal conductivity and aluminum's oxide layer hinder adhesion. To overcome these restrictions, precise control of welding parameters including clamping pressure, vibration amplitude, and welding time requires effective parametric analysis to provide optimal weld energy. Tables 1 and 2 present the mechanical characteristics and chemical composition of the weld specimens.

Table 1. Mechanical properties of Al 6061 and Cu [63]

Properties	Aluminum (Al)	Copper (Cu)
Hardness in HV	40-45	86-89
Elongation in %	14.98	41.03
Tensile Strength in MPa	300-310	230-240

Table 2. Chemical composition of Al 6061 and Cu [63]

Materials	Cu	Fe	Zn	Si	Pb	Al	Ni
Commercial copper	Balance	0.05	4.69	0.009	0.03	0.02	0.03
Al-6061	0.005	0.3	0.005	0.07	0.003	Balance	<0.001

Figure 2 illustrates the welded dissimilar joints. The range of experimental parameters are determined by trial and error based on past experimental findings for the same material, Table 3. Exploratory testing was used to determine the boundary conditions to identify the optimum welding parameter window. Table 4 lists process parameters and joint resistance and strength measurements from these experimental trials.

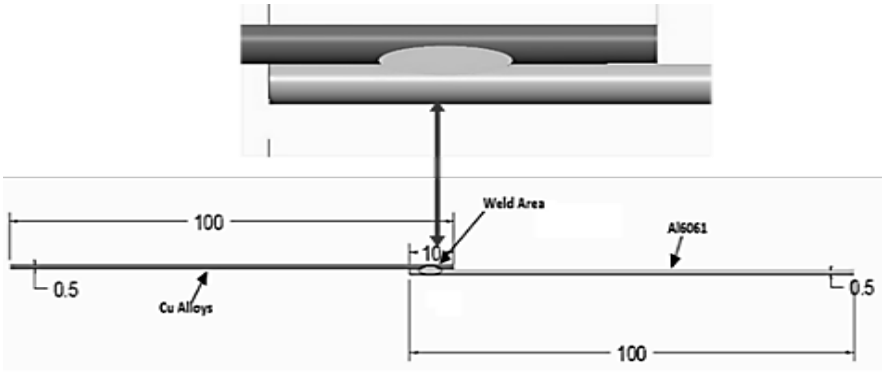

Fig. 2. Cu and Al6061 Lap weld

Table 3. Parameter Levels for Trials

S. No.	Parameters	Level				
		-II	-I	0	I	II
1	Pressure in bar	3.0	3.5	4.0	4.5	5.0
2	welding Time in seconds	1.5	2.0	2.5	3.0	3.5
3	Amplitude in micro-meters	40	45	50	55	60
4	Holding Time in seconds	2	2.5	3	3.5	4

Table 4 Experimental parametric levels and the measured output.

Run	Pressure [bar]	Amplitude [µm]	Weld Time [s]	Holding Time [s]	Joint resistance [Ω]	Strength [MPa]
1	4	50	3.5	3	3.136	1.573
2	4	60	2.5	3	3.0912	1.529
3	4.5	45	2	2.5	3.192	1.21
4	4	50	2.5	2	3.192	1.485
5	4	50	2.5	3	3.64	1.463
6	3.5	55	3	2.5	2.5312	1.375
7	3.5	55	2	2.5	2.3968	1.078
8	5	50	2.5	2.5	2.8672	1.397
9	4.5	55	2	2	2.296	0.99
10	3	50	2.5	2.5	2.5536	1.474
11	4.5	55	2	3.5	2.9344	1.496
12	4	50	2.5	3	3.1584	1.584
13	4	50	2.5	3	3.192	1.595
14	3.5	45	3	3.5	2.3744	1.364
15	4	40	2.5	3	3.36	1.496
16	3.5	45	2	3.5	2.3632	1.045
17	3.5	45	3	2.5	2.464	1.056
18	4.5	55	3	3.5	2.8448	1.518
19	4	50	2.5	3	3.1696	1.562

Run	Pressure [bar]	Amplitude [µm]	Weld Time [s]	Holding Time [s]	Joint resistance [Ω]	Strength [MPa]
20	4.5	45	3	3.5	2.5312	1.155
21	4.5	45	3	2.5	2.5536	1.375
22	4	50	2.5	3	3.024	1.54
23	4	50	1.5	3	2.5536	1.254
24	3.5	45	2	2.5	2.8448	1.045
25	4	50	2.5	4	3.472	1.32
26	3.5	55	2	3.5	2.6208	1.331
27	4	50	2.5	3	3.1472	1.573
28	3.5	55	3	3.5	2.9344	1.232
29	4.5	45	2	3.5	2.5088	1.353
30	4.5	55	3	2.5	2.9344	1.32

The weld specimens were assessed by microscopic examination, mechanical testing, and visual inspections. To evaluate and validate the influence of parametric changes, the weld samples undergo mechanical tests and microscopic imaging. To evaluate the strength of the weld, a shear test is conducted on the wire joints. In addition, SEM, macro, and micro images are taken to assess the structural integrity of the link. Furthermore, the generation of intermetallic compounds (IMCs) at the weld interface is determined using EDAX images. Machine learning technology is used to assess interdependencies among process factors and perform predictive analysis for joint resistance and weld strength. The results and comments section contains the recorded observations and deductions.

3. RESULTS AND DISCUSSION

Figure 3 displays the experimentally welded dissimilar wire junctions of Cu and Al 6061. A visual examination shows an acceptable weld. Shear tensile tests are then run to determine strength, and metallurgical characterizations are also made with the macro and microscopic studies.

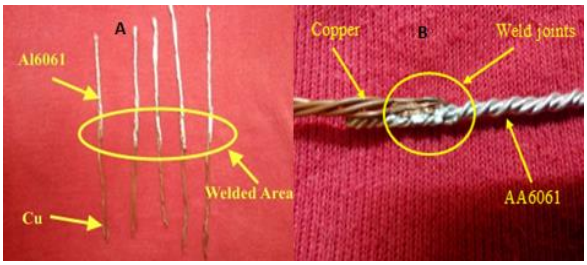

Fig. 3. Ultrasonically welded filaments of dissimilar metals

3.1. Shear Tensile Test

Shear tensile test of the weld specimens is performed to determine the maximum withstanding load for ultrasonically linked wires. The weld specimens have shear strength values that are lower than the base material as listed in Table 4, owing to the geometry of the aluminium and copper wires. The heat input during the ultrasonic welding process also causes a reduction in the strength of the base material. Excessive heat input will result in the deformation of the workpieces. Subsequently, all energy will be allocated towards achieving these deformations, resulting in a reduced amount of energy that can be utilized for the creation of a connection between the metal plates. The measurements also indicate that there is no apparent correlation between the individual factors and the strength of the weld. However, it is necessary to optimize the combination of parameters in order to get the highest possible weld strength.

3.2. Macro-structural Analysis

The wire joint interface's macrostructure is provided by the Al-Cu macrographs, as seen in figure 5. The joint interface shows a clear separation between the two weld specimens, indicating negligible intermetallic at the joint. The Cu molecules are dispersed throughout the Al via mechanical fusion and flow of materials. The joints exhibit thin oxide layers as a result of compressive deformation brought on by ultrasonic vibrations. In the Al/Cu area, bonding is inversely related to welding time. The Al matrix close to the weld interface becomes significantly distorted in the direction of the vibrations due to the formation of micro-bonds between Al and Cu. The Al then developed a recrystallization as seen from the microstructure with a shear pattern.

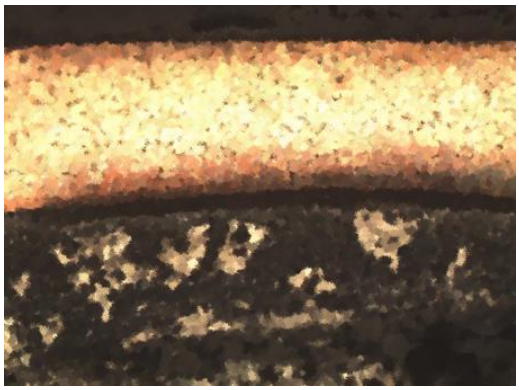

Fig. 5. Macro Image of Al 6061-Cu Weld

3.3. Microstructural Analysis

The optical microscopy image, Figure 6 is analysed for metallographic examination. The weld is subjected to microscopic analysis by immersing it in a solution consisting of 10% ammonia in water that is saturated with hydrogen peroxide for a duration of 20 seconds. The image illustrates the distinct fusion line or HAZ. The HAZ suggests that there is a faster rate of initial heating followed by cooling. Sonotrode penetration depth rises and material thickness decreases with increased welding pressure, leading to an increase in plastic strain. The upper specimen edge has an uneven surface due to high-frequency sonotrode vibration.

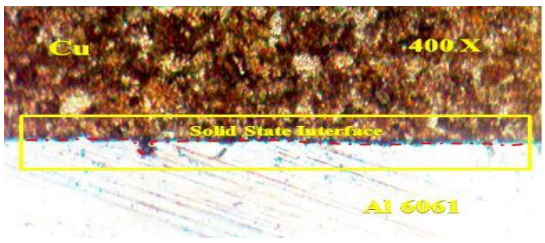

Fig. 6. Microstructural Image at Al 6061-Copper weld

Upon analysing the etched cross-section depicted in Figure 6, an evident contrast can be observed between the copper and aluminum plates. A thin line is commonly found on the etched cross-sections of most welded specimens. This raises the question of whether the plates are interconnected at a metallurgical level or if they are merely compressed in close proximity. In order to assess the presence of an extremely narrow space between the metal plates, a comprehensive examination of the weld interface was carried out utilizing Scanning Electron Microscopy (SEM) and Energy Dispersive X-ray Spectroscopy (EDX).

3.4. Scanning Electron Microscopy and Energy Dispersive X-ray Analysis Results

SEM is used to study the microstructures of fractured specimens. SEM is used to characterize base metals and USW wire junctions to see microstructure changes. Mounted, polished, and etched Al-Cu wire junctions are used for SEM analysis. SEM image, Figure 7, indicates that the joint execution is not uniform since the joint interface is depicted as white. Micro cracks visible in the SEM picture need to be analyzed further to assess their impact on the weld strength. From the picture, there is no continuous fusion zone seen. The concentration gradient region for the Al-Cu wire junction is shown by the white color zone. Using EDX, a line scan is performed to assess the possible presence of an oxide layer at the weld interface. Various elements are detected along a line that is perpendicular to the weld contact by use of this scan. The concentration of Cu, Al, and O at each position along the line is displayed in Figure 7. The parent material elements in the chosen region are displayed in the EDAX results (Fig. 7). For the entire length of the line scan, the oxygen concentration is essentially minimal. At the weld interface, there is no peak in the concentration of oxygen. This indicates that there isn't an oxide layer covering the metal plate surfaces. The Cu and Al lines in both line scans cross over in the vicinity of the weld interface. This suggests that a little amount of mixing occurs between the two components, leading to the formation of a metallurgical connection. As a result, the plates are welded together in addition to being forced together because the metals are different. The fusion zone can contain inter-metallics such as AlCu, Al_2Cu, and Al_4Cu9. It is once more evident from this picture that there was no oxygen concentration found at the weld contact. The weld cross-section contains a trace quantity of oxygen, but it is uniformly distributed across the two metal plates. Due to the oxide layer breaking down during the solid-state welding process, there is a low concentration of oxygen remaining.

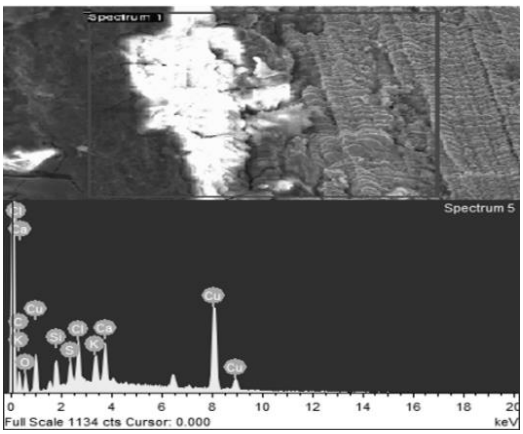

Fig. 7. SEM and EDAX of Al – Cu weld material

The results suggested that as welding energy increases, more plastic deformation occurs along the copper-aluminum weld interface. This is a result of the Cu and Al side of the weld interface softening when the temperature at the Cu alloy and Al 6061 interlayer rises, raising the weld interface temperature.

4. MACHINE LEARNING FOR PARAMETRIC ANALYSIS

Machine learning (ML) is a sophisticated tool capable of predicting the system output when initially trained with the known set of data comprising the input and the corresponding output [64,65]. Table 3 shows the influence of varying levels of independent parameters such as the Pressure, Time, Amplitude, and Holding time on the dependent parameters of weld Strength and Joint resistance. The 75 percent of the data are used for training the module and the remaining data is used for testing. A multiple linear regression algorithm is used for the analysis of four independent variables and two dependent variables. The methodology followed is shown in the flow chart from figure 8.

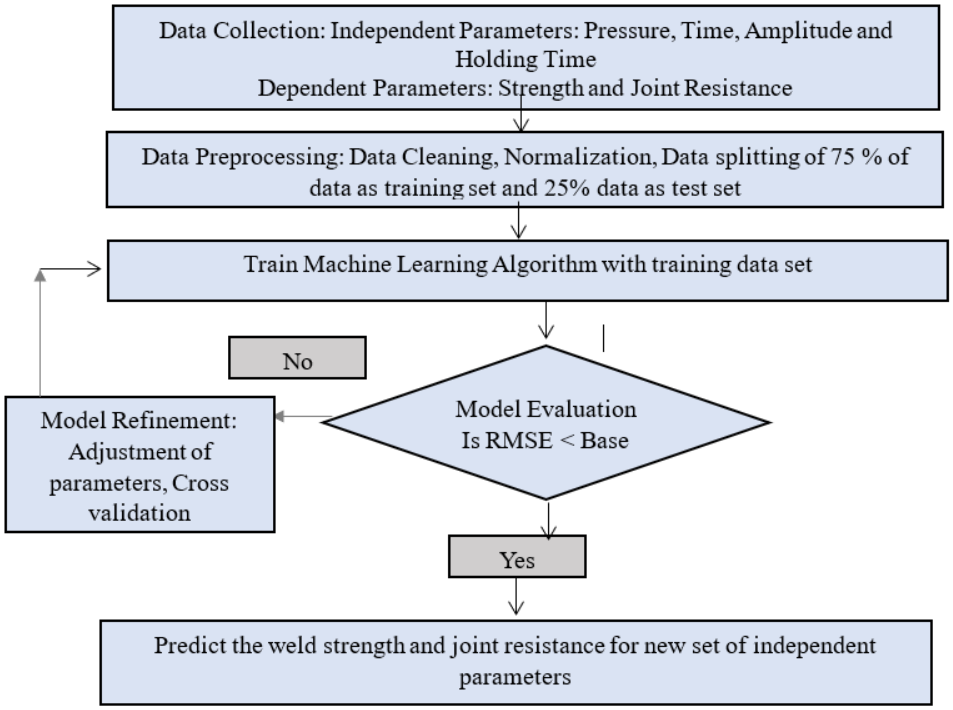

Fig. 8. Flow chart depicting the sequence followed in data analysis using ML algorithm

4.1. Parametric Analysis Results

The predicted values of weld strength for various combinations of input parameters are listed in Table 5. Y_pred is the predicted value for the output parameter strength. Similarly, the predicted values of joint resistance for some parametric combinations are shown in Table 6.

Table 5. Predicted and actual value of the dependent parameter Strength

S.No.	Y_pred	Strength [MPa]
1	1.07	1.10
2	1.16	1.23
3	1.31	1.24
4	1.24	1.36
5	1.23	1.43
6	1.32	1.2
7	1.38	1.12
8	1.23	1.44

Table 6. Predicted and actual value of the dependent parameter Joint resistance

S. No.	y_pred2	Joint resistance [Ω]
1	2.52603	2.85
2	2.5359	2.24
3	2.56689	2.12
4	2.49129	2.62
5	2.52416	2.81
6	2.53402	3.1
7	2.52228	2.62
8	2.52416	2.82

Using the multiple linear regression new values are predicted as shown in Appendix, table A.1, rows 31 to 35. Table A.2 shows the comparison between actual value and predicted value based on multiple regression which clearly shows the algorithm predicts the values very close to the actual value. The multiple linear regression is given by the equation (1):

$$Y = a_1 + a_1 p_1 + a_2 + p_2 + a_3 p_3 + a_4 p_4 \quad (1)$$

Where Y is the dependent parameter, a_0, a_1, a_2, a_3 are the coefficient of the slope and p_1, p_2, p_3 and p_4 are the independent parameter.

The correlation matrix helps estimate the interdependencies of target and process parameters, Table 7. The correlation of holding time, pressure, amplitude, and weld time gives scope for further analysis for the removal of redundant factors, while the high correlation factor between independent and target parameters indicates the strong influence of the process parameter on the result.

Backward elimination regression is utilized for identifying the significant and insignificant parameters among the dependent parameters. Table 8 describes the statistical result for the predicted output. Figure 9 indicates the parameter significance for weld strength and the regression result for parameter significance of joint resistance is shown in figure 10.

Table 7. Correlation between the dependent and independent parameters

Index	Pressure	Time	Amplitude	Holding Time	Strength	Joint Resistance
Pressure	1	6.83E-17	2.18E-17	-0.1095	0.06086	0.1873
Time	6.83E-17	1	7.45E-01	0.69263	0.7829	0.20786
Amplitude	2.18E-17	7.45E-01	1	0.67312	0.74101	0.15921
Holding Time	-1.09E-01	6.93E-01	6.73E-01	1	0.68916	0.31873
Strength	6.09E-02	7.83E-01	7.41E-01	0.68916	1	0.47175
Joint Resistance	1.87E-01	2.08E-01	1.59E-01	0.31873	0.47175	1

Table 8. Statistical Result description for predicted output

Index	Pressure	Time	Amplitude	Holding Time	Strength	Joint Resistance
Count	65	65	65	65	65	65
Mean	4.26923	2.5	50	2.70769	1.35806	2.756448
Std	0.83888	0.60596	6.0596	0.6608	0.20987	0.279021
Min	3	1.5	40	1.5	0.99	2.296
25 %	3.5	2	45	2.5	1.1959	2.5536
50 %	4	2.5	50	3	1.364	2.710947
75 %	4.5	3	55	3	1.52245	2.8672
max	6	3.5	60	4	1.69301	3.64

OLS Regression Results

Dep. Variable:	Strength (N/m2)	R-squared (uncentered):	0.993
Model:	OLS	Adj. R-squared (uncentered):	0.992
Method:	Least Squares	F-statistic:	2073.
Date:	Wed, 14 Feb 2024	Prob (F-statistic):	2.14e-64
Time:	08:59:35	Log-Likelihood:	47.006
No. Observations:	65	AIC:	-86.01
Df Residuals:	61	BIC:	-77.31
Df Model:	4		
Covariance Type:	nonrobust		

	coef	std err	t	P>|t|	[0.025	0.975]
Pressure	0.0346	0.016	2.171	0.034	0.003	0.066
Time (s)	0.1310	0.039	3.343	0.001	0.053	0.209
Amplitude (µm)	0.0139	0.003	5.044	0.000	0.008	0.019
Holding Time (s)	0.0683	0.034	2.006	0.049	0.000	0.136

Omnibus:	6.400	Durbin-Watson:	2.203
Prob(Omnibus):	0.041	Jarque-Bera (JB):	6.123
Skew:	-0.503	Prob(JB):	0.0468
Kurtosis:	4.118	Cond. No.	148.

Fig. 9. Regression result for the dependent variable strength

OLS Regression Results

Dep. Variable:	Joint resistance (Ω)	R-squared (uncentered):	0.985
Model:	OLS	Adj. R-squared (uncentered):	0.984
Method:	Least Squares	F-statistic:	1032.
Date:	Wed, 14 Feb 2024	Prob (F-statistic):	2.97e-55
Time:	09:19:41	Log-Likelihood:	-21.014
No. Observations:	65	AIC:	50.03
Df Residuals:	61	BIC:	58.73
Df Model:	4		
Covariance Type:	nonrobust		

	coef	std err	t	P>|t|	[0.025	0.975]
Pressure	0.2082	0.045	4.589	0.000	0.118	0.299
Time (s)	-0.1522	0.112	-1.364	0.178	-0.375	0.071
Amplitude (µm)	0.0349	0.008	4.441	0.000	0.019	0.051
Holding Time (s)	0.1784	0.097	1.838	0.071	-0.016	0.372

Omnibus:	5.067	Durbin-Watson:	1.720
Prob(Omnibus):	0.079	Jarque-Bera (JB):	4.467
Skew:	0.636	Prob(JB):	0.107
Kurtosis:	3.173	Cond. No.	148.

Fig. 10. Regression result for dependent variable Joint resistance

From the above results it may be seen that pressure, time, and amplitude represent the significant independent parameters but holding Time has P value of 0.049. So, the parameter of holding time is the least significant in predicting the output. The 3D plots in figure 11 to figures 22 show the isolated impact of holding time and amplitude on the weld strength, instead of including all parameters together at once. Weld strength of ultrasonically welded Al-Cu wires is found to decrease with increasing holding time, while the strength is enhanced by higher amplitude (Fig. 11).

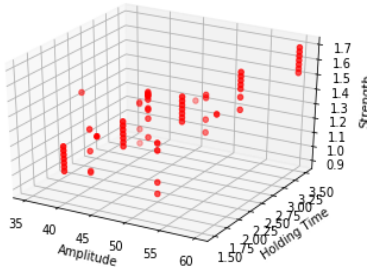

Fig. 11. Feature importance of amplitude vs. holding time

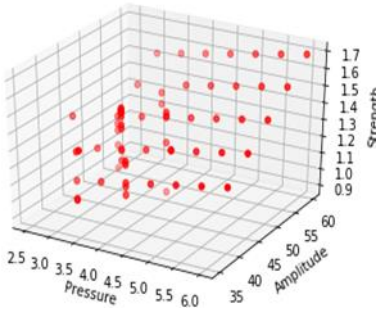

Fig. 12. Feature importance of pressure vs. amplitude

The dependency plot of figure 12 depicts that a rise in both the vibration amplitude and weld pressure to a specific level of 3.5 bar increases the strength. Weld strength is observed to be improved when the weld time is extended and the weld pressure is limited to a specific point (Fig. 13).

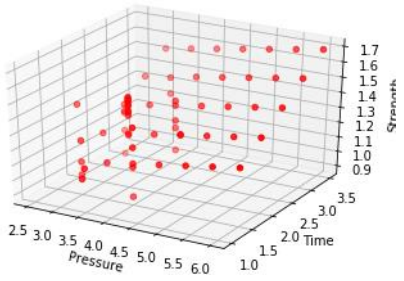

Fig. 13. Feature importance of pressure vs. weld time

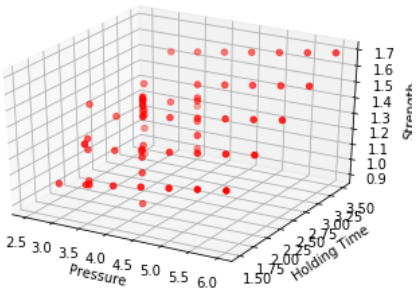

Fig. 14. Feature importance of pressure vs. holding time

Weld strength is improved when weld pressure and holding time are limited to a certain range (Fig. 14). It is depicted in Figure 15 that improving the weld strength requires longer weld times and shorter holding times. According to Figure 16, amplitude has a greater impact on strength than weld duration.

Feature importance and impact on the joint resistance was also studied in the form of 3D dependency plots, which helped to arrive at the hierarchy of independent parameters. Increased holding time and pressure had little effect on joint resistance (Fig. 17). The influence of holding duration and amplitude on joint resistance, where amplitude has a minor effect, is shown in Figure 18. In comparison to amplitude, pressure has a greater influence on joint resistance, Fig. 19. Figure 20 illustrates the finding of enhanced joint resistance for a weld time of 2 s and pressure of 3.5 bar. As compared to holding time, a slight improvement in joint resistance is seen at longer weld times (Fig. 21). As amplitude increases, some progress is shown in terms of joint resistance. The joint resistance is not improved by the weld time, Figure 22.

Based on the dependency plots, the influence of the process parameters on the weld strength and joint resistance is summarised as in Table 9.

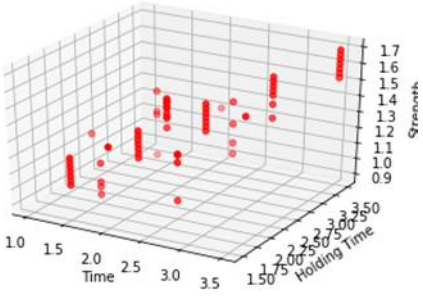

Fig. 15. Feature importance of weld time vs. holding time

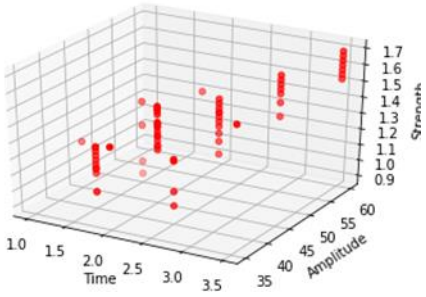

Fig. 16. Feature importance of time for weld vs amplitude

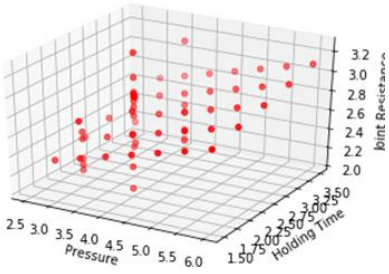

Fig. 17. Feature importance of pressure vs. holding time

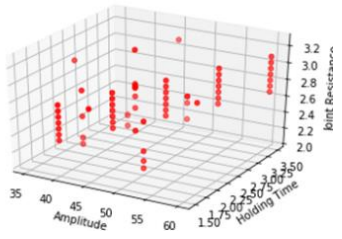

Fig. 18. Feature Importance of Amplitude vs. Holding Time

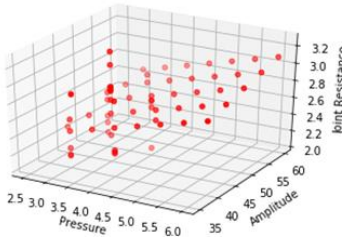

Fig. 19. Feature importance of pressure vs. amplitude

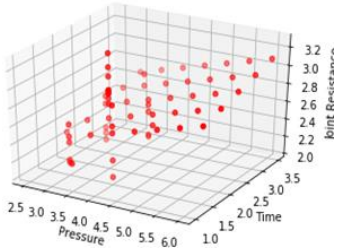

Fig. 20. Feature importance of pressure vs. welding time

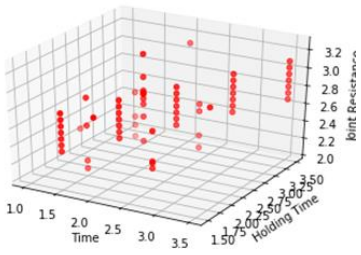

Fig. 21. Feature importance of welding time vs. holding time

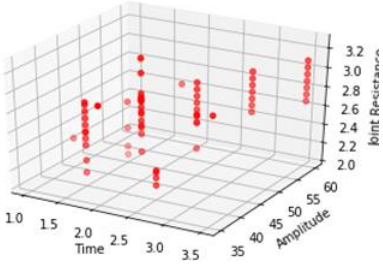

Fig. 22. Feature importance of welding time vs. amplitude

Table 9. Feature Importance Summarised from the 3D Dependency plots

Parameter	Joint Strength		Joint Resistance	
	Direct/Inverse Effect	**Range for Good Result**	**Direct/Inverse Effect**	**Range for Good Result**
Pressure	Direct	Up to specific value	Direct	Up to specific value
Amplitude	Direct	Material Dependent	Direct	Material dependent
Weld Time	Direct	Material Dependent	Direct	Up to specific value
Hold time	Inverse	Up to specific value	Direct	Material dependent

5. CONCLUSIONS

This study presents a comprehensive analysis of the mechanical behaviour and microstructural characteristics of Al-Cu dissimilar wire joints welded using the ultrasonic joining process, commonly applied in automotive components, heat exchangers, and electrical appliances. Experiments were performed with systematic variation of key process parameters, namely vibration amplitude, pressure, weld time and hold time. The analysis primarily focused on metallurgical transformations, evaluating molecular diffusion patterns, diffusion consistency, and resulting strength alterations due to ultrasonic vibrational heat. This was followed by multiple regression machine learning techniques for parametric analysis. The results obtained are as follows:

- The lap shear tensile strength has a direct correlation with welding energy.
- The presence of the alloy particle interlayer significantly impacts the mechanical properties.
- The study of both macro and micro structures demonstrates strong bonding and integrity.
- High weld time and amplitude and optimal holding time and pressure increase the weld strength as also recorded from the parametrical predictions performed with machine learning.
- An indication of the quality of the weld can also be obtained from the measured electrical joint resistance, which revealed that the existence of the unbonded component at the interface reflected a higher joint resistance.

The study of ultrasonic joining of Al-Cu dissimilar wire joints demonstrates important progress in our comprehension of the mechanical behavior and microstructural properties. The study shows enhanced weld strength and consistency by investigating metallurgical transformations and improving process parameters, with implications for better design of automobile, heat exchanger, and electrical applications.

Subsequent investigations in this field have the potential to greatly improve the comprehension, utilization, and sustainability of ultrasonic welding in various industrial contexts. Longevity and robustness can be better understood by looking into the long-term performance and dependability of ultrasonic welded joints in various environmental settings. Advanced characterization methods at the nano and microscale, such as transmission electron microscopy (TEM) and atom probe tomography (APT), can provide more detailed understanding of bonding and diffusion processes at the atomic level. Furthermore, combining ultrasonic welding with other methods—like laser welding or adhesive bonding—can result in hybrid procedures that combine the best features of many approaches for improved joint performance.

REFERENCES

[1] **Shakil M., Tariq N. H., Ahmad M., Choudhary M. A., Akhter J. I., Babu S. S.,** *Effect of ultrasonic welding parameters on microstructure and mechanical properties of dissimilar joints. Materials & Design*, vol. 55, pp. 263-273, 2014.

[2] **Yang J. W., Cao B., He X. C., Luo H. S.,** *Microstructure evolution and mechanical properties of Cu–Al joints by ultrasonic welding. Science and Technology of Welding and Joining*, vol. 19, iss. 6, pp. 500-504, 2014.

[3] **Balasundaram R., Patel, V.K., Bhole S.D., Chen D.L**., *Effect of zinc interlayer on ultrasonic spot-welded aluminium-to-copper joints. Materials Science and Engineering*: A, vol. 607, pp. 277-286, 2014.

[4] **Ji H., Wang, J., Li M.,** *Evolution of the bulk microstructure in 1100 aluminium builds fabricated by ultrasonic metal welding. Journal of Materials Processing Technology*, vol. 214, iss. 2, pp.175-182, 2014.

[5] **Fujiia H. T., Goto Y., Sato Y. S., Kokawa H.,** *Microstructural evolution in dissimilar joint of Al alloy and Cu during ultrasonic welding*, in Materials Science Forum, April 2014.

[6] **Zhang C. Q., Robson J. D., Ciuca O., Prangnell P. B**., *Microstructural characterization and mechanical properties of high power ultrasonic spot welded aluminium alloy AA6111–TiAl6V4 dissimilar joints*, Materials Characterization, vol. 97, pp.83-91, 2014.

[7] **Macwan A., Chen D. L**., *Microstructure and mechanical properties of ultrasonic spot-welded copper-to-magnesium alloy joints.* Materials & Design, vol. 84, pp. 261-269, 2015.

[8] **Patel V. K., Bhole S. D., Chen D. L**., *Ultrasonic spot welding of aluminum to high-strength low-alloy steel: microstructure, tensile and fatigue properties*, Metallurgical and Materials Transactions A, vol. 45, iss. 4, pp. 2055-2066, 2014.

[9] **Sasaki T., Nagai T., Watanabe T**., *Analysis of ultrasonic welding process of mild steel and 5052 aluminium alloys*, Welding International, pp.1-8, 2017.

[10] **Satpathy M. P., Sahoo S. K., Datta S.**, *Acoustic horn design and effects of process parameters on properties of dissimilar ultrasonic welding aluminium to brass*, Materials and Manufacturing Processes, vol. 31, iss. 3, pp. 283-290, 2016.

[11] **Wu X., Liu T., Cai W**., *Microstructure, welding mechanism, and failure of Al/Cu ultrasonic welds*, Journal of Manufacturing Processes, vol. 20, pp. 321-331, 2015.

[12] **Yang J., Cao B.**, *Investigation of resistance heat assisted ultrasonic welding of 6061 aluminum alloys to pure copper*, Materials & Design, vol. 74, pp. 19-24, 2015.
[13] **Seok S. J., Jang H. S., Park D. S.,** *Ultrasonic welding of Ni and Cu sheets*, Materials and Manufacturing Processes, vol. 30, iss. 9, pp. 1069-1073, 2015.
[14] **Lee S. S., Kim T. H., Hu S. J., Cai W. W., Abell J. A.**, *Analysis of weld formation in multilayer ultrasonic metal welding using high-speed images*, Journal of Manufacturing Science and Engineering, vol. 137, iss. 3, p.031016, 2015.
[15] **Zhang G., Takahashi Y., Heng Z., Takashima K., Misawa K.,** *Ultrasonic weldability of Al ribbon to Cu sheet and the dissimilar joint formation mode*, Materials Transactions, vol. 56, iss. 11, pp.1842-1851, 2015.
[16] **Satpathy M. P., Moharana B. R., Dewangan S., Sahoo S. K.**, *Modeling and optimization of ultrasonic metal welding on dissimilar sheets using fuzzy based genetic algorithm approach*, Engineering Science and Technology, vol. 18, iss. 4, pp. 634-647, 2015.
[17] **Haddadi F., Abu-Farha F.**, *Microstructural and mechanical performance of aluminium to steel high power ultrasonic spot welding*, Journal of Materials Processing Technology, vol. 225, pp. 262-274, 2015.
[18] **Mirza F. A., Macwan A., Bhole S. D., Chen D. L., Chen X. G.**, *Microstructure, tensile and fatigue properties of ultrasonic spot welded aluminium to galvanized high-strength-low-alloy and low-carbon steel sheets*, Materials Science and Engineering: A, vol. 690, pp. 323-336, 2017.
[19] **Asami, T., Miura, H.**, *Ultrasonic welding of dissimilar metals by vibration with planar locus*. Acoustical Science and Technology, 36(3), pp.232-239, 2015.
[20] **Jedrasiak P., Shercliff H. R., Chen Y. C., Wang L., Prangnell P., Robson J.**, *Modeling of the thermal field in dissimilar alloy ultrasonic welding*, Journal of Materials Engineering and Performance, vol. 24, iss. 2, pp. 799-807, 2015.
[21] **Kicukov E., Gursel A.**, *Ultrasonic welding of dissimilar materials: A review*, Periodicals of Engineering and Natural Sciences (PEN), vol. 3, iss. 1, 2015.
[22] **Shin H. S., de Leon M.**, *Parametric study in similar ultrasonic spot welding of A5052-H32 alloy sheets*, Journal of Materials Processing Technology, vol. 224, pp. 222-232, 2015.
[23] **Xu L., Wang L., Chen Y. C., Robson, J. D., Prangnell P.B.**, *Effect of interfacial reaction on the mechanical performance of steel to aluminum dissimilar ultrasonic spot welds*, Metallurgical and Materials Transactions A, vol. 47, iss. 1, pp. 334-346, 2016.
[24] **Ni Z., Zhao H., Mi P., Ye F.,** *Microstructure and mechanical performances of ultrasonic spot welded Al/Cu joints with Al 2219 alloy particle interlayer*, Materials & Design, vol. 92, pp. 779-786, 2016.
[25] **Satpathy M. P., Sahoo S. K.,** *Microstructural and mechanical performance of ultrasonic spot welded Al–Cu joints for various surface conditions*, Journal of Manufacturing Processes, vol. 22, pp. 108-114, 2016.
[26] **Zhang C. Q., Robson, J. D., Prangnell P. B.**, *Dissimilar ultrasonic spot welding of aerospace aluminum alloy AA2139 to titanium alloy TiAl6V4*, Journal of Materials Processing Technology, vol. 231, pp. 382-388, 2016.
[27] **Sridharan N., Wolcott P., Dapino M., Babu S. S.**, *Microstructure and texture evolution in aluminum and commercially pure titanium dissimilar welds fabricated using ultrasonic additive manufacturing*. Scripta Materialia, vol. 117, pp. 1-5, 2016.
[28] **Shen N., Samanta A., Ding H., Cai W. W.,** *Simulating microstructure evolution of battery tabs during ultrasonic welding*. Journal of Manufacturing Processes, vol. 23, pp. 306-314, 2016.
[29] **Higashi Y., Iwamoto C., Kawamura Y.,** *Microstructure evolution and mechanical properties of extruded Mg 96 Zn 2 Y 2 alloy joints with ultrasonic spot welding*. Materials Science and Engineering: A, vol. 651, pp. 925-934, 2016.
[30] **Chen K., Zhang Y., Wang H.,** *Effect of acoustic softening on the thermal-mechanical process of ultrasonic welding*, Ultrasonics, vol. 75, pp. 9-21, 2017.
[31] **Satpathy M. P., Sahoo S. K.**, *An experimental investigation on joining of aluminium with steel using ultrasonic metal welding*, International Journal of Mechatronics and Manufacturing Systems, vol. 9, iss. 4, pp. 299-309, 2016.
[32] **Banu M., Hu S. J., Cai W., Abell J.,** *Performance Prediction for Ultrasonically Welded Dissimilar Materials Joints*, Ann Arbor, 1001, p. 48109, 2017.
[33] **Satpathy M. P., Sahoo S. K.,** *Mechanical performance and metallurgical characterization of ultrasonically welded dissimilar joints*. Journal of Manufacturing Processes, vol. 25, pp. 443-451, 2017.
[34] **Ni Z. L., Ye F. X.**, *Dissimilar Joining of Aluminum to Copper Using Ultrasonic Welding*, Materials and Manufacturing Processes, vol. 31, iss. 16, pp. 2091-2100, 2016.
[35] **Deng Q., Fu R., Jing L., Wang Y.,** *Influence of cold-rolling and annealing treatments on microstructure and mechanical properties of friction stir-welded Al–Cu joints*, Science and Technology of Welding and Joining, vol. 21, iss. 8, pp. 614-623, 2016.
[36] **Ni Z. L., Ye F. X.**, *Weldability and mechanical properties of ultrasonic joining of aluminium to copper alloy with an interlayer*, Materials Letters, vol. 182, pp. 19-22, 2016.
[37] **Zhou X., Zhang G., Shi Y., Zhu M., Yang F.,** *Microstructures and mechanical behavior of aluminum-copper lap joints*, Materials Science and Engineering: A, vol. 705, pp. 105-113, 2017.
[38] **Haddadi F.,** *Microstructure reaction control of dissimilar automotive aluminium to galvanized steel sheets ultrasonic spot welding*. Materials Science and Engineering: A, vol. 678, pp. 72-84, 2016.
[39] **Asami T., Miura H., Ueoka T., Tsujino J., Tip W., Hongoh M., Iwase E., Tsuboi H.,** *Ultrasonic metal welding with a vibration source using longitudinal and torsional vibration transducers*, Japanese Journal of Applied Physics, vol. 56, p. 07JE02, 2017.
[40] **Asami T., Tamada Y., Higuchi Y., Miura H.,** *Development of dumbbell-shape vibration source with longitudinal and torsional transducers for ultrasonic metal welding*, Ultrasonics Symposium (IUS), IEEE International, pp. 1-4, 2017.
[41] **Bergmann J. P., Regensburg A., Schürer R., Petzoldt F., Herb A.,** *Effect of the interface characteristics on the joint properties and diffusion mechanisms during ultrasonic metal welding of Al/Cu*, Welding in the World, vol. 61, iss. 3, pp. 499-506, 2017.
[42] **Lee S. S., Kim T. H., Hu S. J., Cai W., Abell J. A., Li J.,** *Defining Joint Quality Using Weld Attributes in Ultrasonic Welding of Lithium-Ion Batteries*, ASME Press, 2017.
[43] **Kang, B., Cai, W., Tan, C.A.**, *Fundamental Dynamics of Ultrasonic Welding. In Ultrasonic Welding of Lithium-Ion Batteries*. ASME Press, 2017.
[44] **Lionetto F., Balle F., Maffezzoli A.**, *Hybrid ultrasonic spot welding of aluminum to carbon fiber reinforced epoxy composites*. Journal of Materials Processing Technology, vol. 247, pp. 289-295, 2017.
[45] **Lee S. S., Shao C., Kim T. H., Hu S. J., Kannatey-Asibu E., Cai W., Spicer J. P., Abell J.A.,** *Process Monitoring Using Online Sensor Signals In Ultrasonic Welding of Lithium-Ion Batteries*, ASME Press, 2017
[46] **Regensburg A., Petzoldt F., Schürer R., Hellwig P., Bergmann J. P.,** *Effect of local preheating during ultrasonic welding of Al-Cu joints on strand compaction and bond formation*. Welding in the World, vol. 61, iss. 3, pp. 443-451, 2017.
[47] **Regensburg A., Petzoldt F., Schürer R., Hellwig P., Bergmann J. P.**, *Effect of local preheating during ultrasonic welding of Al-Cu joints on strand compaction and bond formation*, Welding in the World, vol. 61, iss. 3, pp. 443-451, 2017.
[48] **Li J., Monaghan T., Nguyen T. T., Kay R. W., Friel R. J., Harris R. A.,** *Multifunctional metal matrix composites with embedded printed electrical materials fabricated by ultrasonic additive manufacturing*, Composites Part B: Engineering, vol. 113, pp. 342-354, 2017.
[49] **Khan U., Khan N. Z., Gulati J.**, *Ultrasonic Welding of Bi-Metals: Optimizing Process Parameters for Maximum Tensile-Shear Strength and Plasticity of Welds*, Procedia Engineering, vol. 173, pp.1447-1454, 2017.
[50] **Zhang Z., Wang K., Li J., Yu Q., Cai W.,** *Investigation of Interfacial Layer for Ultrasonic Spot Welded Aluminum to Copper Joints*, Scientific reports, vol. 7, iss. 1, p.12505, 2017.
[51] **Zhang H. M., Chao Y. J., Luo Z.,** *Effect of interlayer on microstructure and mechanical properties of Al–Ti ultrasonic welds*, Science and Technology of Welding and Joining, vol. 22, iss. 1, pp. 79-86, 2017.

[52] **Yang J., Cao B., Lu Q.,** *The effect of welding energy on the microstructural and mechanical properties of ultrasonic-welded copper joints*, Materials, vol. 10, iss. 2, p.193, 2017.
[53] **Peng H., Chen D., Jiang X.,** *Microstructure and Mechanical Properties of an Ultrasonic Spot Welded Aluminum Alloy: The Effect of Welding Energy*, Materials, vol. 10, pp. 5, p. 449, 2017.
[54] **Satpathy M. P., Mohapatra K. D., Sahoo S. K.,** *Ultrasonic spot welding of Al–Cu dissimilar metals: a study on parametric influence and thermo-mechanical simulation*, International Journal of Modelling and Simulation, pp. 1-13, 2017.
[55] **Liu G., Hu X., Fu Y., Li Y.,** *Microstructure and Mechanical Properties of Ultrasonic Welded Joint of 1060 Aluminum Alloy and T2 Pure Copper*, Metals, vol. 7, iss. 9, p. 361, 2017.
[56] **Liu J., Cao B., Yang J.,** *Effects of Vibration Amplitude on Microstructure Evolution and Mechanical Strength of Ultrasonic Spot-Welded Cu/Al Joints*, Metals, vol. 7, iss. 11, p. 471, 2017.
[57] **Shin H. S., de Leon M.,** *Mechanical performance and electrical resistance of ultrasonic welded multiple Cu-Al layers*, Journal of Materials Processing Technology, vol. 241, pp. 141-153, 2017.
[58] **Macwan A., Kumar A., Chen D. L.,** *Ultrasonic spot welded 6111-T4 aluminum alloy to galvanized high-strength low-alloy steel: Microstructure and mechanical properties*, Materials & Design, vol. 113, pp. 284-296, 2017.
[59] **Ren D., Zhao K., Pan M., Chang Y., Gang S., Zhao D.,** *Ultrasonic spot welding of magnesium alloy to titanium alloy*, Scripta Materialia, vol. 126, pp. 58-62, 2017.
[60] **Satpathy M. P., Kumar A., Sahoo S. K.**, *Effect of Brass Interlayer Sheet on Microstructure and Joint Performance of Ultrasonic Spot-Welded Copper-Steel Joints*, Journal of Materials Engineering and Performance, vol. 26, iss. 7, pp. 3254-3262, 2017.
[61] **Balogh M. P., Cai W. W., Rinker T. J., Chapaton T. J., Lu P., Hartnagle E. G.,** *Elimination of tool adhesion in an ultrasonic welding process*, U.S. Patent 9,573,221, 2017.
[62] **Mostafavi S., Hesser D. F., Markert B.,** *Detection of terminal oscillation pattern in ultrasonic metal welding*, Journal of Manufacturing Processes, vol. 41, pp. 159-167, 2019.
[63] **Mohan Raj N., Kumaraswamidhas L.A., Nalajam P.K. et al.,** *Studies on Electro Mechanical Aspects in Ultrasonically Welded Al/Cu Joints*, Transactions of the Indian Institute of Metals, vol. 71, pp. 107-116, 2018.
[64] **Michie D., Spiegelhalter D. J., Taylor C. C.,** *Machine learning*, Neural and Statistical Classification, vol. 13, pp. 1-298, 1994.
[65] **Pedregosa F., Varoquaux G., Gramfort A., Michel V., Thirion B., Grisel O., Blondel M., Prettenhofer P., Weiss R., Dubourg V., Vanderplas J**., *Scikit-learn: Machine learning in Python*, Journal of Machine Learning Research, vol. 12 (oct.), pp. 2825-2830, 2011.
[66] **Cai W., Wang J., Jiang P., Cao L., Mi G., Zhou Q.,** *Application of sensing techniques and artificial intelligence-based methods to laser welding real-time monitoring: A critical review of recent literature*, Journal of Manufacturing Systems, vol. 57, pp. 1-18, 2020.
[67] **Eren B., Guvenc M. A., Mistikoglu S.,** *Artificial intelligence applications for friction stir welding: A review*, Metals and Materials International, vol. 27, pp. 193-219, 2021.
[68] **Tsuzuki R.**, *Development of automation and artificial intelligence technology for welding and inspection process in aircraft industry*, Welding in the World, vol. 66, iss. 1, pp. 105-116, 2022.
[69] **Cardellicchio A., Nitti M., Patruno C., Mosca N., di Summa M., Stella E., Renò V.,** *Automatic quality control of aluminium parts welds based on 3D data and artificial intelligence*, Journal of Intelligent Manufacturing, pp.1-20, 2023.

APPENDIX

A.1 Predicted value using multiple linear regression [From 31 to 65]

Run	Pressure [bar]	Time [s]	Amplitude [µm]	Holding Time [s]	Strength [MPa]	Joint resistance [Ω]
31	3	1.5	40	1.5	1.02	2.42
32	3	2	45	2	1.18	2.46
33	3	2.5	50	2.5	1.34	2.51
34	3	3	55	3	1.50	2.56
35	3	3.5	60	3.5	1.66	2.61
36	3.5	1.5	40	1.5	1.02	2.47
37	3.5	2	45	2	1.18	2.51
38	3.5	2.5	50	2.5	1.34	2.56
39	3.5	3	55	3	1.50	2.61
40	3.5	3.5	60	3.5	1.66	2.66
41	4	1.5	40	1.5	1.03	2.52
42	4	2	45	2	1.19	2.56
43	4	2.5	50	2.5	1.35	2.61
44	4	3	55	3	1.51	2.66
45	4	3.5	60	3.5	1.67	2.71
46	4.5	1.5	40	1.5	1.03	2.57
47	4.5	2	45	2	1.19	2.61
48	4.5	2.5	50	2.5	1.35	2.66
49	4.5	3	55	3	1.51	2.71
50	4.5	3.5	60	3.5	1.67	2.76
51	5	1.5	40	1.5	1.03	2.61
52	5	2	45	2	1.20	2.66
53	5	2.5	50	2.5	1.36	2.71

Run	Pressure [bar]	Time [s]	Amplitude [μm]	Holding Time [s]	Strength [MPa]	Joint resistance [Ω]
54	5	3	55	3	1.52	2.76
55	5	3.5	60	3.5	1.68	2.80
56	5.5	1.5	40	1.5	1.04	2.66
57	5.5	2	45	2	1.20	2.71
58	5.5	2.5	50	2.5	1.36	2.76
59	5.5	3	55	3	1.52	2.81
60	5.5	3.5	60	3.5	1.68	2.85
61	6	1.5	40	1.5	1.04	2.71
62	6	2	45	2	1.21	2.76
63	6	2.5	50	2.5	1.37	2.81
64	6	3	55	3	1.53	2.86
65	6	3.5	60	3.5	1.69	2.90

A.2 Comparison of predicted value with actual value

Strength [MPa]			Joint resistance [Ω]		
Predicted	Actual	Error %	Predicted	Actual	Error %
1.02	1	2	2.42	2.1	15.2381
1.18	1.2	-1.66667	2.47	2.21	11.76471
1.34	1.42	-5.6338	2.52	2.82	-10.6383
1.5	1.49	0.671141	2.56	2.82	-9.21986
1.66	1.67	-0.5988	2.61	2.72	-4.04412
1.02	1	2	2.47	2.65	-6.79245
1.18	1.2	-1.66667	2.52	2.81	-10.3203
1.35	1.35	0	2.57	2.82	-8.86525
1.51	1.45	4.137931	2.61	2.8	-6.78571
1.67	1.67	0	2.66	2.83	-6.00707
1.03	1	3	2.52	2.72	-7.35294
1.19	1.8	-33.8889	2.57	2.67	-3.74532
1.35	1	35	2.62	2.74	-4.37956
1.51	1.49	1.342282	2.66	2.77	-3.97112
1.67	1.59	5.031447	2.71	2.78	-2.51799
1.04	1.1	-5.45455	2.57	2.84	-9.50704
1.19	1	19	2.62	2.9	-9.65517
1.36	1.34	1.492537	2.67	2.91	-8.24742
1.52	1.67	-8.98204	2.71	3	-9.66667
1.68	1.68	0	2.76	3.1	-10.9677
1.04	1.1	-5.45455	2.62	2.94	-10.8844
1.21	1.2	0.833333	2.67	2.93	-8.87372
1.36	1.33	2.255639	2.71	2.9	-6.55172
1.52	1.4	8.571429	2.76	2.87	-3.83275
1.68	1.5	12	2.81	3.12	-9.9359
1.04	1.1	-5.45455	2.67	2.96	-9.7973
1.21	1.58	-23.4177	2.72	2.98	-8.72483
1.36	1.4	-2.85714	2.76	2.92	-5.47945
1.53	1.49	2.684564	2.81	3.1	-9.35484

Strength [MPa]			Joint resistance [Ω]		
Predicted	**Actual**	**Error %**	**Predicted**	**Actual**	**Error %**
1.68	1.7	-1.17647	2.86	3.12	-8.33333
1.05	1.1	-4.54545	2.72	3.14	-13.3758
1.21	1.21	0	2.76	3	-8
1.37	1.36	0.735294	2.81	3.2	-12.1875
1.53	1.52	0.657895	2.86	3.1	-7.74194
1.69	1.61	4.968944	2.91	3.2	-9.0625